Automated measurement of epidermal thickness from optical coherence tomography images using line region growing

Jomer Delacruz, Jesse Weissman, Kirk Gossage

Jomer Delacruz, Jesse Weissman, Kirk Gossage, "Automated measurement of epidermal thickness from optical coherence tomography images using line region growing," Proc. SPIE 7548, Photonic Therapeutics and Diagnostics VI, 75480E (2 March 2010); doi: 10.1117/12.842353

SPIE.

Event: SPIE BiOS, 2010, San Francisco, California, United States

Automated Measurement of Epidermal Thickness from Optical Coherence Tomography Using Line Region Growing

Jomer Delacruz[a], Jesse Weissman[a], Kirk Gossage[a]
[a]Unilever HPC, 40 Merritt Blvd., Trumbull, CT, USA 06611;

ABSTRACT

Optical Coherence Tomography (OCT) is a non-invasive imaging modality that acquires cross sectional images of tissue in-vivo. It accelerates skin diagnosis by eliminating invasive biopsy and laborious histology in the process. Dermatologists have widely used it for looking at morphology of skin diseases such as psoriasis, dermatitis, basal cell carcinoma etc. Skin scientists have also successfully used it for looking at differences in epidermal thickness and its underlying structure with respect to age, body sites, ethnicity, gender, and other related factors.

Similar to other in-vivo imaging systems, OCT images suffer from a high degree of speckle and noise content, which hinders examination of tissue structures. Most of the previous work in OCT segmentation of skin was done manually. This compromised the quality of the results by limiting the analyses to a few frames per area.

In this paper, we discuss a region growing method for automatic identification of the upper and lower boundaries of the epidermis in living human skin tissue. This image analysis method utilizes images obtained from a frequency-domain OCT. This system is high-resolution and high-speed, and thus capable of capturing volumetric images of the skin in short time. The three-dimensional (3D) data provides additional information that is used in the segmentation process to help compensate for the inherent noise in the images. This method not only provides a better estimation of the epidermal thickness, but also generates a 3D surface map of the epidermal-dermal junction, from which underlying topography can be visualized and further quantified.

Keywords: OCT, segmentation, region growing, epidermis

1. INTRODUCTION

The thickness of the epidermal layer of the skin has long been linked to a youthful and healthy skin appearance. Epidermal thickening, as a product-induced benefit, has been observed from various active ingredients such as retinoic acid treatment– see Figure 1[1]. Currently, investigation of epidermal thickness is done through collection of biopsies by a board-certified dermatologists and subsequent histology. This process is not only resource intensive but also limits panelist participation in these clinical studies. In addition, the removal of the skin takes away the opportunity to evaluate product efficacy over time on the same skin site. Therefore, there is a significant interest in the development of a non-invasive method for the measurement of epidermal thickness.

Optical coherence tomography (OCT) is a non-invasive imaging modality that acquires cross sectional images of tissue in-vivo. It has accelerated skin diagnosis by eliminating the time and resource shortcomings of the histology process as previously mentioned. Dermatologists have widely used it in looking at the morphology of skin diseases such as psoriasis, dermatitis, basal cell carcinoma, etc. Skin scientists have also successfully used it for looking at the differences in the epidermal thickness and its underlying structure with respect to age, body site, ethnicity, gender, and other related factors [2].

Photonic Therapeutics and Diagnostics VI, edited by N. Kollias, B. Choi, H. Zeng, R. S. Malek, B. J.-F. Wong, J. F. R. Ilgner, K. W. Gregory, G. J. Tearney, L. Marcu, H. Hirschberg, S. J. Madsen, A. Mandelis, A. Mahadevan-Jansen, E. D. Jansen, Proc. of SPIE Vol. 7548, 75480E · © 2010 SPIE · CCC code: 1605-7422/10/$18 · doi: 10.1117/12.842353

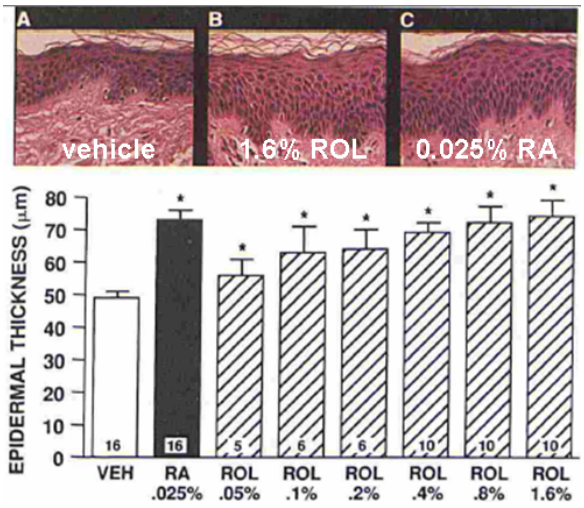

Figure 1. Retinoic acid promotes epidermal thickening

The OCT system collects volumetric images of the skin tissue by first doing sequential scanning in the x direction (B-scan) with a fixed depth in the z direction (A-scan). Then, repeating the same process as it scans in the y direction. The system renders an image volume with high-quality contrast in the z-axis, which makes it ideal for looking at the skin surface and dermal-epidermal junction (DEJ). Nonetheless, similar to other in-vivo imaging systems based on coherent light sources, OCT images suffer from a high degree of speckle and noise content, which hinders the examination of tissue structures.

Most of the previous work in OCT segmentation of skin was done manually. This compromised the quality of the results by limiting the analysis to a few frames per area rather than using a large enough number of frames to form a sufficient volume. In order to take full advantage of the data acquired from the OCT each individual slice in the image has to be considered for the analysis. Automated image analysis (IA) of OCT images has been explored in the past, which attempts to fully automate the analysis and the extraction of relevant information from the OCT slices.

A previous segmentation attempt using a shapelet-based technique was utilized by Weissman et al [3]. In this method, isotropic Gaussian kernels of different dilations were used as basis functions for the shapelets. Each shapelet image was calculated through the convolution of the magnitudes and directions of the images and shapelet kernel's gradients, and the skin surface was detected by a column-wise search for local minima. Then, the stratum corneum (SC) and DEJ boundaries were detected by running a 3X3 median window and looking for the first minimum and first maximum in each A-scan column. Depending on the length scale the midpoint was taken either as the SC or DEJ position. The final boundaries were obtained by applying least median of squares statistics.

Hori et. al. looked mainly at the intensity values of the image [4]. First, the image was blurred with a 5x5 median filter then intensity peaks were detected to delineate the skin surface. A 6^{th} order polynomial fitting was used to smooth the line across the A-scan (one frame). Then, the same procedure was applied independently in all the frames. Another 6^{th} order polynomial was applied perpendicularly across the frames to achieve a smooth 3D surface. Finally, the DEJ was delineated by running a 3X3 moving average of the A-scan and detecting a local minimum intensity below the delineated skin surface. Another 6^{th} order polynomial was applied to smooth the final DEJ outline.

Zakharov et al. used similar approach by looking at image intensity [5]. Analogous to the above methods, they first established the skin surface. Next, they flattened out the image with respect to the surface, and then the average of all the A-scans was computed. Finally looking at the laterally–averaged profile, they detect the first minimum and first maximum, from which the midpoint was established and considered as the DEJ boundary.

In this paper, we discuss a region growing method for automated identification of the upper and lower boundaries of the epidermis in living human skin tissue. This IA method utilizes images obtained from a spectral-domain OCT. This

system is of high-resolution and high-speed, and is thus capable of capturing volumetric images of the skin in a short period of time with minimal motion artifacts. This technique makes use of the three-dimensional (3D) data of the OCT to compensate for the inherent noise in the images during the segmentation process. Subsequently, the epidermal thickness is calculated from the 3D surfaces of upper (skin surface) and lower (DEJ) boundaries. This method not only provides a better estimation of the epidermal thickness, but also generates a 3D surface map of the DEJ from which the underlying topography can be visualized and further quantified.

2. MATERIALS AND METHODOLOGY

2.1. Overview

The OCT volumetric image was obtained from a spectral domain OCT (SD-OCT) system manufactured by Thorlabs (Newton, NJ). It consisted of a series of individual OCT frames collected at different spatial locations (Figure 2). The axis orientation with respect to the image volume in Figure 2 will be used throughout this paper. Compared to the older time-domain OCT systems, the SD-OCT is of higher speed and is capable of image capture rates of 30-60 frames per second (fps) (depending on the pixel resolution in the x-direction) thus allowing for high-quality volumetric imaging of the skin. In addition, the system is of higher resolution which enables a resolving power of 7.2 μm and 3.2 μm in the X-Y and Z planes respectively, with a maximum imaging depth of 2.2mm within the skin. This improvement in the technology allows for the investigation of the underlying structures in more detail, yielding better measurements.

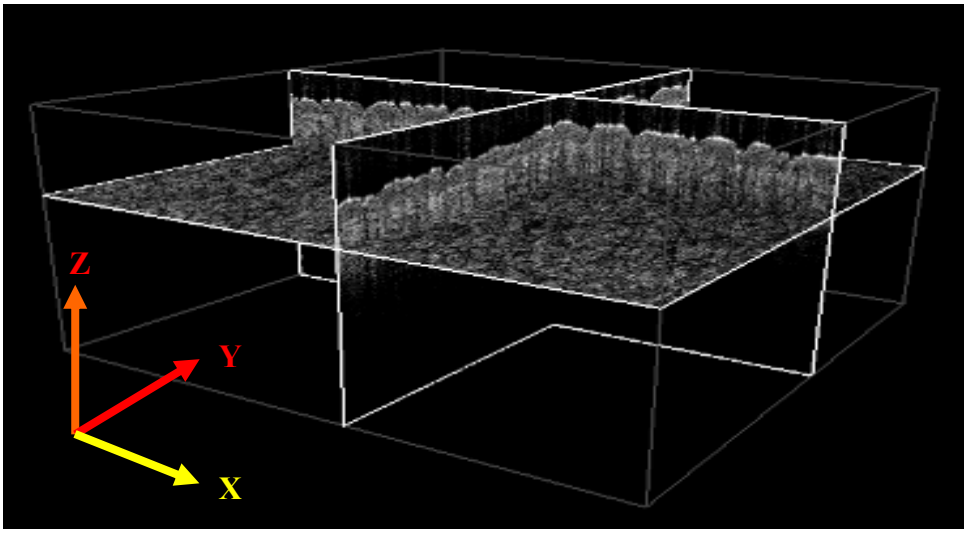

Figure 2. OCT volumetric image shown with Thorlabs OCT viewer.

The image processing method was developed to primarily segment the skin epidermis, from which its thickness was measured. This was achieved by morphologically delineating its upper and lower boundaries. The following section describes the image processing routine used for the segmentation of both the skin surface and DEJ boundaries. The process was broken down into three stages which include image pre-processing, region growing, and epidermal thickness calculation.

2.2. Image Pre-processing

2.2.1. Noise and speckle reduction

The image data collected from OCT systems are highly notorious for the amount of embedded speckle and noise. The speckles mainly emanate from the coherent light source used in the system due to interference in the back scattered light. The noise was driven by the imaging components themselves (detectors) and the dynamic settings (auto gain) etc. In addition, undesired components in the image such as hair reflectance, motion artefacts, etc. were considered as features that needed to be accounted for in the clean up process. In this effect, individual frames were first pre-processed to reduce noise and speckle. This was effectively achieved with the use of Speckle Reducing Anisotropic Diffusion (SRAD) (6). This method is the multi-scale extension of the edge-sensitive Frost and Lee smoothing filters that removes both noise and speckle. Since SRAD is a time-dependent, multi-scale operation, it circumvents any arbitrary filter kernel size parameterization. This is achieved by going through all possible length-scales with the diffusion process until convergence is achieved, see Figure 3.

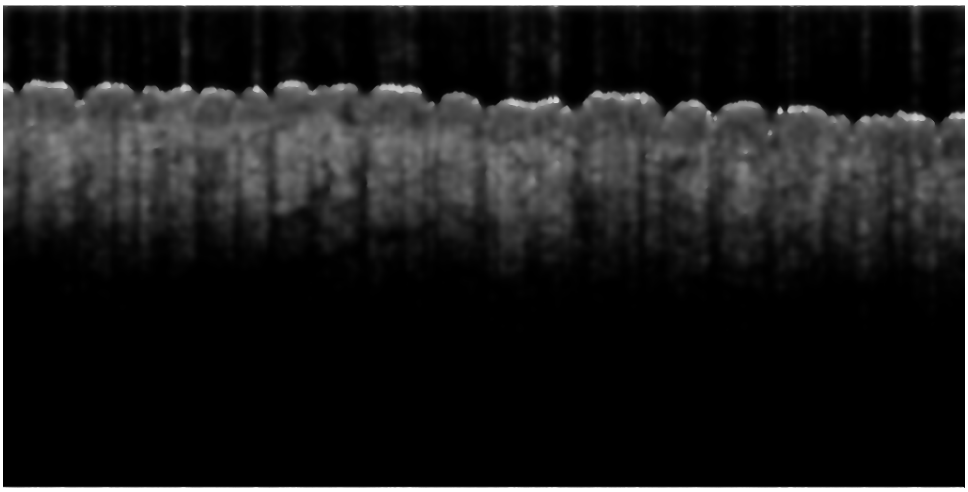

Figure 3. Low pass filtering using SRAD.

2.2.2. Gradient Calculation

After the noise/speckle reduction process, the gradient of the image was calculated. Gradient operation is an edge detection algorithm that operates independently in x and z directions. The refractive indices mismatch between air and skin as well as between epidermis and dermis present prominent intensity contrast at their respective boundaries, this information was the main image feature used in the segmentation. The gradient not only highlights these boundaries in the image but also provides edge extensions necessary for the subsequent operations. Also, OCT images have prominent vertical boundaries, which arise from either biological structure (hair, follicles, etc) in the skin and/or exposure differences among blocks of A-scans. Regardless of the source, these boundaries were not of high importance and interfere in the delineation process. Therefore, the gradient in the z-direction was only utilized in the analysis (Figure 4).

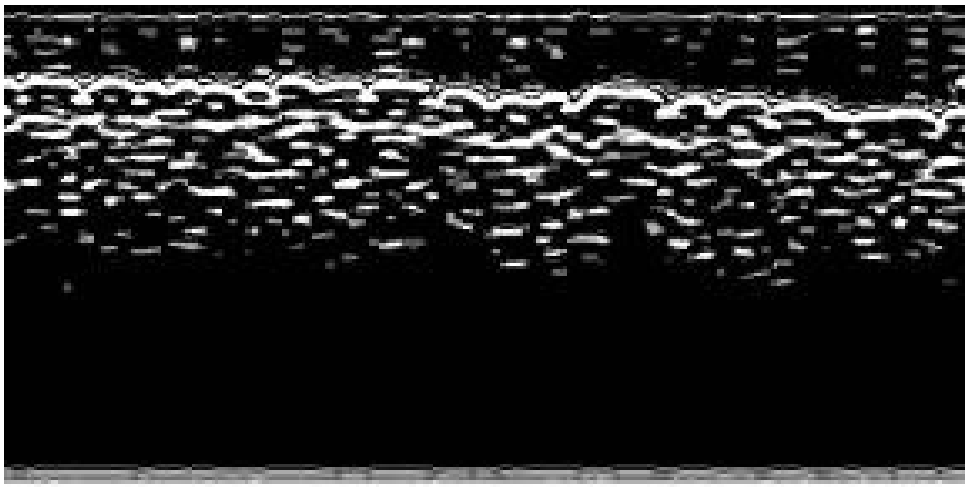

Figure 4. Gradient image in z-direction

2.2.3. Distance Transform

The final step of image preparation was the distance transform. Prior to transformation, the image was subjected to component removal based on the area and eccentricity. The components in the gradient image have sufficient information to effectively perform this operation. This processing further removes unwanted components that may interfere in the subsequent operation. Afterwards, the distance transform was applied, which provides the necessary image for the edge-based region growing technique (Figure 5).

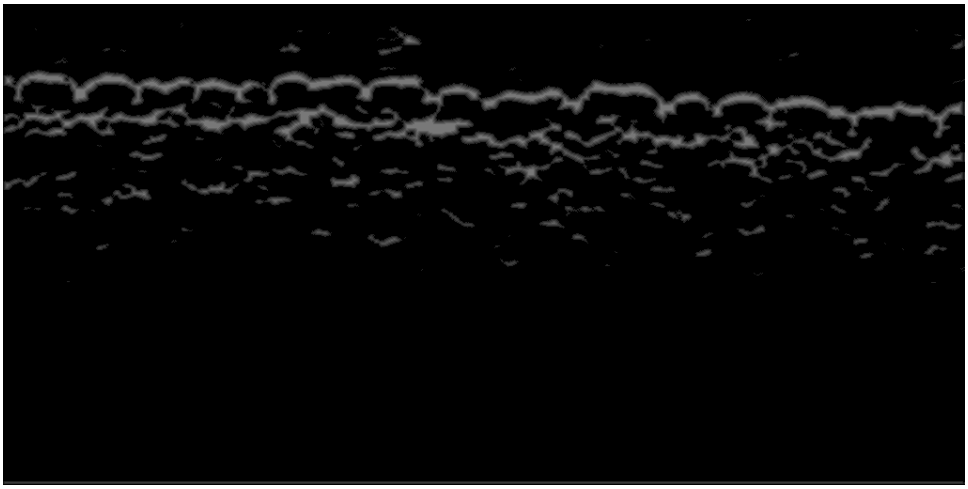

Figure 5. Distance transformed image

2.3. The Region Growing

2.3.1 Peak Detection

An initial estimation of the boundaries was done through a column-wise peak detection algorithm. First, the peaks that correspond to the skin surface boundary were detected. Then these peaks were used as offsets to the next boundary line (DEJ). This way, the lines that correspond to the surface would not be considered for the detection of DEJ line. Due to the presence of persistent undesired features in the image, even after the pre-processing, the detected peaks may not necessarily correspond to the actual boundaries. This was remedied in the subsequent operations, namely, the seeding.

2.3.2. Seeding

Region growing is based on the placement of points (seeds) from which the branches grow. In the normal region growing method, the properties of the starting seeds dictate the conditions to grow the branches. Therefore, the success of the technique is highly dependent on the initial placement of the seeds and the number of the seeds. For this purpose we devised a procedure to disperse the seeds on the OCT image by taking a polynomial fit of the initial peaks calculated above. Afterwards, the seeds were then placed along the fit line (Figure 6). Since the fit line does not necessarily coincide with the actual boundary, the seeds were therefore allowed to move to the closest boundary before growing. A total of 250 seeds were used for each line (skin surface and DEJ).

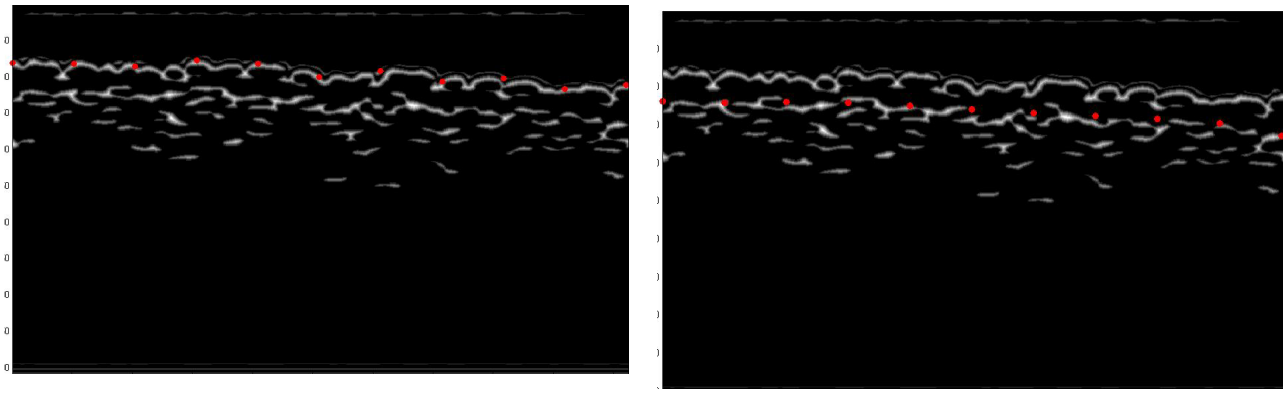

Figure 6. Seeds placement on skin surface and DEJ boundaries – 11 of 250 seeds are shown.

2.3.3. Growing

In this paper, we devised an edge-based line region growing scheme that separated the regions of interest rather than segmenting the regions themselves. This edge-based, line region growing was accomplished by following the path that corresponded to the local maximum as initiated by the seed. This local maximum represented the local boundary as discussed above. By tracing this maximum, in a column-wise fashion across the image, it allowed the whole boundary to be delineated. In this paper, the growing procedure was restricted by allowing each x-value to have only one corresponding z-value, which rendered a monotonic line. The method generated two monotonic lines; where the first line corresponded to the boundary between the air and skin regions, and the second line corresponded to the boundary between the epidermis and the dermis regions. The line region R used to grow the i_{th} seed s from its left and right sides was formulated as follows:

$$R^{s_i}_{x+t,z+h}$$

where

$$t = [-seed\_\text{int}erval .. -2 .. -1 .. 0 .. 1 .. 2 .. seed\_\text{int}erval] \tag{1}$$

and

$$h = \begin{cases} -z_{\max} & if\ \max_z([v_{z-n}...v_{z-1}, v_z, v_{z+1}...v_{z+n}]) < z \\ 0 & if\ \max_z([v_{z-n}...v_{z-1}, v_z, v_{z+1}...v_{z+n}]) = z \\ z_{\max} & if\ \max_z([v_{z-n}...v_{z-1}, v_z, v_{z+1}...v_{z+n}]) > z \end{cases} \quad where \quad v_{z\pm n} = \sum_{x=0}^{N} I_{x,z\pm n}$$

Where ***N*** and ***n*** starting values were ***±3*** and ***±5*** respectively. These starting values for ***N*** and ***n*** did not necessarily guarantee a maximum. This happened whenever discontinuations in the boundary occurred, which were highly likely in OCT images. In order to circumvent this, ***N*** and ***n*** were allowed to dynamically increase by 1 until a maximum value was found. Nonetheless, ***N*** was first exhausted before ***n*** was increased by 1, the whole process was repeated until a maximum was found. The ***N*** iteration was limited to 10 while the ***n*** iteration was limited to 35. In addition, the growing in the ***x*** direction was limited to the ± ***seed interval***. The reasoning behind this will be discussed in the following section.

2.3.4. Two-Dimensional Line Merging

The number of line regions, R^s, generated from the line growing was equal to the number of seeds ***s***. Thus, these lines needed to be merged into a single line that constituted the segmented boundary. The line merging process through out the length (***x***-direction) of the image was done as follows:

$$R^{2D-final}_{x,z} = \frac{R^{s_{i\geq x}}_{x,z} + R^{s_{i+1\leq x}}_{x,z}}{2} \tag{2}$$

As mentioned, the line branching from each seed was restricted to grow monotonically in the ***x*** direction to the ± seed interval. Allowing the seed to grow to the entire width of the image caused the line merging process to be heavily weighted by the number of lines that took the same path. In effect, a path that was not necessarily a valid one may end up in the final merged line. This happened very frequently in highly noisy OCT images, which resulted in very poor, unreliable boundary segmentation. Thus, limiting the growth to ± ***seed interval*** in the ***x*** direction allowed a path to be delineated only by two different lines branching from two different seeds. This provided an opportunity for 50/50 cross-checking for the validity of the boundary by calculating the average coordinates of the two region lines R^s and R^{s+1}. The point, $R^{2D-final}_{x,z}$, of the final line represented the same path taken by the two growing lines, which was most likely to be the valid region boundary; otherwise, it was the average of the two lines points.

2.3.5. Three-dimensional Refinement of Skin Surface and DEJ Lines

The line region growing method discussed above was performed simultaneously on three frames of the OCT images in order to do a final line 3D refinement. Due to a high degree of noise in the image, the information provided by a single

frame was not enough to obtain reliable segmentation. This 3D refinement allowed for cross-checking between frames and facilitated more reliable boundary segmentation, significantly improving the robustness of finding the valid boundaries. Also, it provided more refined, smoother 3D reconstruction of the skin surface and DEJ, which, in turn, provided a better estimate of 3D epidermal thickness (Figure 7).

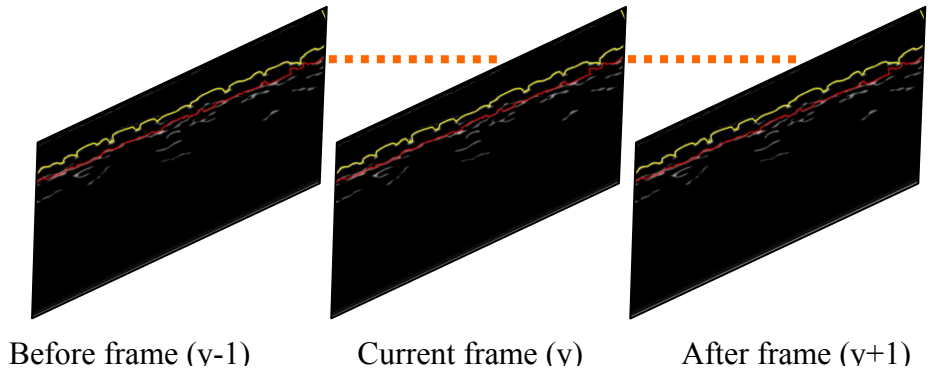

Figure 7. Frames y-1, y, and y+1 used for 3D refinement of the surface and DEJ boundary lines.

The 3D refinement was normally done by taking the point-wise average of three lines from each frame. Yet in some scenarios, this yielded false results if any of the lines happened to have points that were incorrectly segmented. In order to circumvent this, the final 3D surface, $R^{3D-final}$, was obtained as follows,

$$R_{x,y,z}^{3D-final} = \begin{cases} \dfrac{R_{x,y-1,z}^{2D-final} + R_{x,y,z}^{2D-final}}{2} & if \quad diffBC < Z_{limit}, \quad diffCA > Z_{limit}, \quad diffBA > Z_{limit} \\ \dfrac{R_{x,y,z}^{2D-final} + R_{x,y+1,z}^{2D-final}}{2} & if \quad diffCA < Z_{limit}, \quad diffBC > Z_{limit}, \quad diffBA > Z_{limit}, \\ \dfrac{R_{x,y-1,z}^{2D-final} + R_{x,y+1,z}^{2D-final}}{2} & if \quad diffBA < Z_{limit}, \quad diffBC > Z_{limit}, \quad diffCA > Z_{limit}, \\ \dfrac{R_{x,y-1,z}^{2D-final} + R_{x,y,z}^{2D-final} + R_{x,y+1,z}^{2D-final}}{3} & if \quad diffBC < Z_{limit} \quad diffCA < Z_{limit} \quad diffBA < Z_{lim} \end{cases}$$

where

$$diffBC = \left| R_{x,y-1,z}^{2D-final} - R_{x,y,z}^{2D-final} \right|$$

and

$$diffCA = \left| R_{x,y,z}^{2D-final} - R_{x,y+1,z}^{2D-final} \right| \tag{3}$$

and

$$diffBA = \left| R_{x,y-1,z}^{2D-final} - R_{x,y+1,z}^{2D-final} \right|$$

and

$$Z_{\lim it} = 10$$

The Z_{limit} was the restriction in z-axis to further prevent the inclusion of false boundary driven by noise. Figure 8 shows the skin surface and DEJ boundary lines after 3D refinement on a single frame. Apart from the first and last slice, the whole process was performed on the rest of the frames of an OCT volume. The final outcomes were 3D boundaries of skin surface and DEJ.

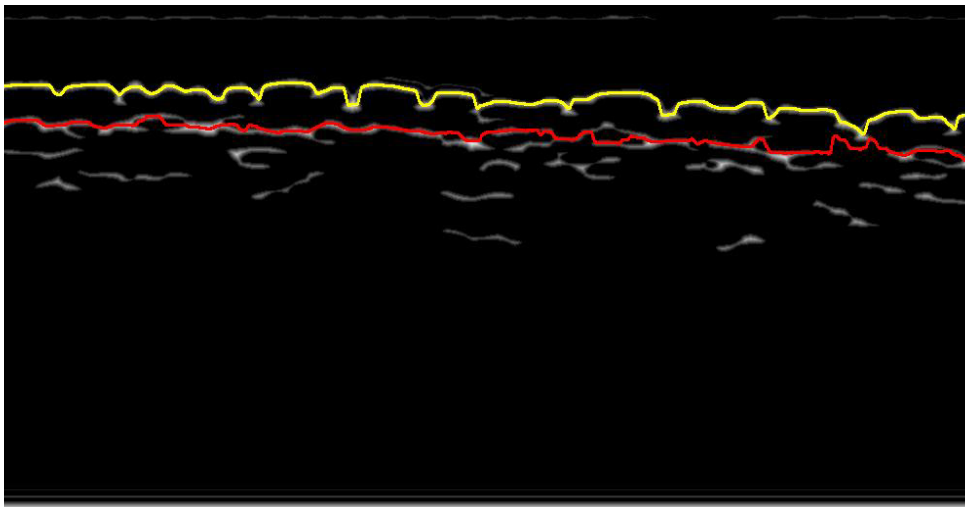

Figure 8. Skin surface and DEJ boundaries after 3D refinement.

2.4. Epidermal Thickness Calculation

The epidermal thickness was calculated by taking the difference of ***z***-coordinates between the two monotonic skin surface (***RSS***) and DEJ (***RDEJ***) lines. A single number was reported by taking the average of the thickness in the ***y***- and ***x***-directions, which represented the 3D epidermal thickness. The calculation was done as follows:

$$Epidermal\_Thickness = \frac{\sum_{y=1}^{length} \sum_{x=1}^{width} RSS_{x,y,z}^{3D-final} - RDEJ_{x,y,z}^{3D-final}}{length * width} \tag{4}$$

The normal *length* and *width* of an image volume are 512 frames and 1024 pixels.

2.5. Multi-threaded Programming

As is seen, an ensemble of image processing algorithms were used to achieve the final segmentation. Each of these methods contributes to the total time-complexity of the whole process. Particularly in the region growing, the quality of the final segmentation was correlated to the amount of starting seeds. However, additional seeds add to the total time-complexity. Since, a normal OCT dataset consisted of 512 images, it was essential to limit the time of overall image processing. Therefore, the algorithm was designed to take advantage of parallel computation capability of both the CPU and GPU. This not only allowed for the use of the time-consuming multi-scale technique, SRAD, but also allowed for the use of many seeds for the skin surface and DEJ line delineation. With multi-threaded programming, the processing time of a 512-image volume was decreased to approximately 10 minutes.

3. RESULTS AND DISCUSSION

The results of the segmentation using the new method are shown in Figure 9. Figure 9a shows a single frame of the OCT image volume overlaid with the skin surface (yellow) and DEJ lines (red) – both boundaries were satisfactorily delineated. Even with a monotonic line, the curvature of the skin surface was properly captured. The DEJ boundary line also showed some degree of curvature. This indicated that the egg-carton-like structure of the DEJ may have been partially captured and delineated. Nonetheless, validation needs to be performed. The strength of the method lies on the fact that 3D information was used to improve the definition of the boundaries. This made the segmentation robust over noise and motion artifacts and also allowed for smooth 3D boundary reconstructions. Figure 9b and Figure 9c are the 3D reconstructions of the skin surface and DEJ respectively derived from the 1048 OCT frames. Looking particularly at the skin surface, the segmentation technique successfully captured its topography with good detail (Figure 9b). This opens an opportunity for an objective, texture-based characterization of skin surface – similar to that obtained from a surface profilometry technique. Even with some motion (dark bands) artifacts, the segmentation process was able to extract the boundaries successfully. The 3D surface of the DEJ (Figure 9c) also displayed some degree of texture. This texture was driven by the inherent anatomy of the DEJ boundary. Nonetheless, a 3D egg-carton-like structure was not observed in any of the constructed images due mainly to the magnification limit of the OCT system used for acquisition. See **Error! Reference source not found.**Appendix 1 for more results.

The epidermal thickness measurements of frontal forearms from four healthy subjects are shown on Table 1 – one OCT volume per subject. Interestingly, the calculated 3D thicknesses were higher than the usual range of 60-100μm for the arm. One of the possible explanations for this came from the fact that most of the reported thicknesses from literature were calculated from either a single slice or a few slices. With the natural variability in the skin, even within common areas, it is not surprising that the numbers reported would be different due to the small number of slices. Here, the calculated thickness value was based on the full 3D data set which should provide a more accurate measure of skin epidermal thickness. In addition, many of the reported skin thicknesses came from histological measurements. This process may have introduced embedding and sectioning artifacts to the tissue, which will both act to underestimate/overestimate the thickness of the skin. Another possible explanation of the thickness difference could be due to the resolution of the new OCT system. The boundary captured by the method described here may have embodied the lower boundary of the DEJ. If this was the case, the overall thickness will always be overestimated.

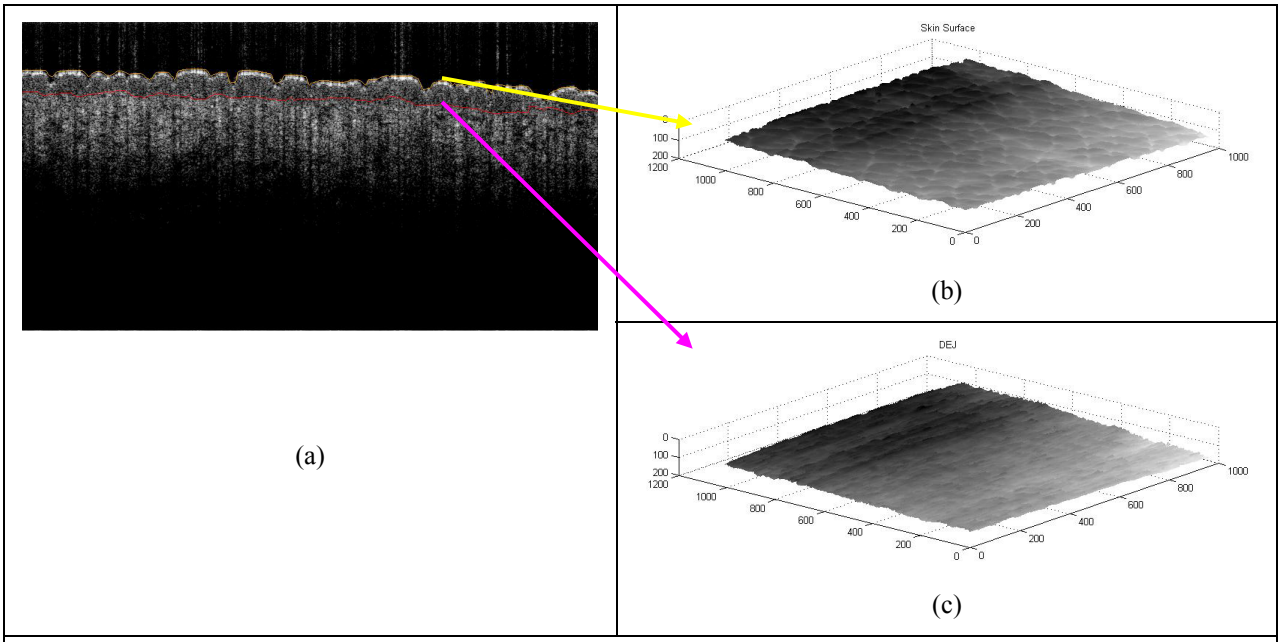

Figure 9. A single OCT frame (a) and respective skin surface (b) and epidermal-dermal junction (c)

Table 1 . Epidermal thickness from the ventral forearms of four volunteers

Subjects	Gender	Body Part	Average 3D Thickness(±STD) (μm)
1	F	ventral forearm	116.6 (±19.6)
2	M	ventral forearm	126.4 (± 18.3)
3	M	ventral forearm	119.1 (±19.0)
4	M	ventral forearm	97.6 (±14.2)

4. CONCLUSIONS

The primary objective of this work was to develop a robust, fast, and viable automated measurement of epidermal thickness from a non-invasive OCT system that can replace biopsies and thus speed up the turn-around time for clinical studies evaluating changes in epidermal thickness. A new approach based on a region growing technique was explored for the segmentation of epidermis, from which the thickness was calculated. The method was fully automated and designed to take advantage of the capability of multi-core machines and the GPU for faster program execution. The method described in this work has been proven to efficiently segment the skin surface and DEJ boundaries. In addition, it was able to provide a smooth 3D reconstruction of the skin surface and DEJ boundaries from the noisy and speckled OCT images with embedded motion artifacts. These two surfaces allowed the calculation of epidermal thickness over the entire x and y dimensions, which provided a more realistic representation of the actual thickness than any single-frame

measurement. In addition, compared to other techniques, the texture information of the constructed surface was retained. The 3D surface offers an opportunity for an objective texture measurement of the skin surface; similar to that of a surface profilometry technique.

REFERENCES

[1] Kang S., Duell E.A., Fisher G.J., Datta S.C., Wang Z.-Q., Reddy A.P., Tavakkol A., Yi Y., Griffiths C.E.M., Elder J.T., Voorhees J.J., "Application of retinol to human skin in vivo induces epidermal hyperplasia and cellular retinoid binding proteins characteristic of retinoic acid but without measurable retinoic acid levels or irritation." J. Invest. Dermatol. 105, 549– 556 (1995).

[2] Bernard Querleux1, The´re`se Baldeweck1, Ste´phane Diridollou2, Jean de Rigal.. "Skin from various ethnic origins and aging: an in vivo cross-sectional multimodality imaging study." Skin Research and Technology; 15: 306–313 (2009)

[3] Jesse Weissman, Tom Hancewicz, and Peter Kaplan, "Optical coherence tomography of skin for measurement of epidermal thickness by shapelet-based image analysis." Optics Express, 12(23), 5760-5769 (2004).

[4] Yasuaki Hori, Yoshiaki Yasuno, "Automatic characterization and segmentation of human skin using three-dimensional optical coherence tomography." Optics Express, 14(5), 1862-1877 (2006).

[5] P. Zakharov1, M.S. Talary1, I. Kolm2, A. Caduff, "Rapid Skin Profiling with Non-Contact Full-Field Optical Coherence Tomography: Study of Patients with Diabetes Mellitus Type I." Biomedical Optics, SPIE 7372, 73720G (2009)

[6] Yu Y. and Acton S., "Speckle reducing anisotropic diffusion." IEEE transaction on image processing, 11(11),1260-1270 (2002).

[7] James Varani*, Elizabeth A. Kelley, Patricia Perone, Humaira Lateef. "Retinoid-induced epidermal hyperplasia in human skin organ culture: inhibition with soy extract and soy isoflavones." Experimental and Molecular Pathology 77, 176– 183 (2004)